Improved lunar edge response function for on-orbit modulation transfer function calibration using albedo flattening

James N. Caron* **and Chris J. Rollins**
Research Support Instruments, Lanham, Maryland, United States

Abstract. The resolution of an imaging system can be quantified using the modulation transfer function (MTF) derived from an image with an edge feature. For Earth-viewing satellites, imaging an appropriate terrestrial edge feature is difficult when optical blur from the atmosphere contaminates the MTF. With a sharp edge and no atmosphere, our Moon has provided researchers with an alternative by deriving the line spread function from the lunar edge. The Moon's surface, however, has features, e.g., craters and seas, that depart from clean step-like behavior, making curve fitting to the data difficult and diminishing the effectiveness of the method. We demonstrate an improvement in which a reflectance (albedo) map of the Moon, created from a mosaic of the U.S. Department of Defense/NASA Clementine images, is used to flatten the surface features before the edge spread function is measured. The objective is to improve the reliability of MTF measurements for on-orbit calibration of the National Oceanic and Atmospheric Administration/NASA Geostationary Operational Environmental Satellite (GOES) weather satellites and similar missions. The technique is applied to the reflective bands of the Advanced Baseline Imager on GOES-16 and GOES-17 weather monitoring satellites. © *2020 Society of Photo-Optical Instrumentation Engineers (SPIE)* [DOI: 10.1117/1.JRS.14.032408]

Keywords: modulation transfer function; calibration; image processing; flat field; weather satellite.

Paper 190576SS received Jul. 26, 2019; accepted for publication May 21, 2020; published online Jun. 4, 2020.

1 Introduction

The spatial resolution of an imaging system can be quantified by deriving the modulation transfer function (MTF) as the Fourier transform of the spatial derivative of an edge feature in an image[1] (International Standard ISO 12233:2017). This diagnostic can be accomplished in a laboratory setting by imaging a scene with an edge feature that is neither perpendicular nor parallel to the sensor axis, but this is difficult to achieve for Earth-viewing satellites. Li et al.[2] and Nelson et al.[3] have used edge features on Earth to estimate the MTF for orbiting cameras, but atmospheric turbulence complicated the measurement.[4] The resulting MTF is a function of both the optical system and the propagation of the light through the nonstatic atmosphere at the time of capture.

This issue can be avoided by imaging the illuminated sharp edge of the Moon. This approach was used by Shea et al.[5] in 1999 to derive the MTF in both vertical and horizontal directions for the NASA/National Oceanic and Atmospheric Administration (NOAA) Geostationary Operational Environmental Satellite (GOES)-N program. The lunar edge response was recorded again in 2014 to monitor the performance of the Moderate resolution Imaging Spectroradiometer (MODIS) on-board the Terra and Aqua satellites,[6] the Lunar Reconnaissance Orbiter Wide Angle Camera in 2016,[7] the Advanced Himawari Imager camera on the Himawari-8 satellite in 2017,[8] and the Advanced Baseline Imager (ABI) on GOES-16 in 2019.[9] The lunar features located near the edge, mainly craters and seas, being spatially variegated,[10] reduce the effectiveness of the approach by disrupting the form of an ideal step function. The reliability of the

*Address all correspondence to James N. Caron, E-mail: Caron@RSImd.com

1931-3195/2020/$28.00 © 2020 SPIE

measurement can be improved if the local albedo variations of lunar features can be diminished while not impacting the MTF measurement.

In this paper, the albedo-variation features of the Moon are reduced by dividing out a reflectance (albedo) map of the Moon, derived from the U.S. Department of Defense (DoD)/NASA Clementine images,[11] from lunar images captured by the ABI[12] on the GOES-16 and GOES-17 satellites. The albedo flattening (AlF) process involves aligning the reflectance map by iterative application of phase correlation to match the Clementine image to the position and orientation of the Moon in the ABI image. The result of the operation is a relatively featureless moon image that can be used to measure the edge spread function (ESF).

2 Representative Images

The ABI is a 16-channel passive imaging radiometer whose highest resolution channel is a 1×1380 pixel array that scans across a two-dimensional scene.[12] Created for the GOES-R series of environmental monitoring satellites, the imager was launched on GOES-16 (November 19, 2016) and GOES-17 (March 1, 2018). Images of the Moon are captured periodically, providing an opportunity for calibration of the sensors. When viewing Earth, the imager produces 0.5-km pixel resolution in band 2, 1-km pixel resolution in bands 1, 3, and 5, and 2-km pixel resolution in band 4. Band 1 has a pixel angle of 22.04×10^{-6} rad, producing a spatial pixel resolution on the Moon of 9.26 km/pixel. The ABI image shown in Fig. 1(a) was taken from the first band with a wavelength of 0.47 μm on February 17, 2017, and it is used in this paper to demonstrate this technique.

ABI images have several levels of calibration, from raw (level 0) to calibrated and navigated detector data resampled into pixels in the fixed grid (level 1b).[13] The resampling process depends on image interpolation and can adversely affect the resolution measurement. Our process is applied to images at the level 1α with calibrated detector samples in radiance units in a swath but not yet resampled to a fixed grid. Pixel values of level 1α images have a band-averaged spectral radiance with units of $\mathrm{mW}/(\mathrm{m}^2\,\mathrm{sr}\,\mathrm{cm}^{-1})$.[13]

The Clementine lunar mapper, a joint space venture between the Ballistic Missile Defense Organization and NASA, was launched in 1994 to test spacecraft components under extended space exposure and obtain multispectral images of the entire lunar surface. The Clementine imaging system consisted of a telescope, a 6-channel filter wheel, an image intensifier, and frame-transfer CCD.[14] The image array had 288×384 pixels, providing a pixel resolution between 7 and 20 m. Figure 1(b) is a revised reflectance map with a center wavelength of 750 nm created by stitching images from the medium resolution ultraviolet/visible camera together.[15,16]

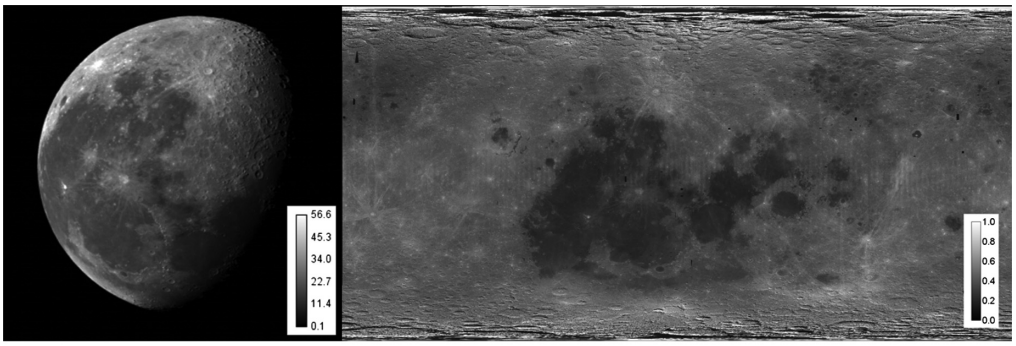

(a) (b)

Fig. 1 (a) Example of an ABI image (band 1), taken on February 17, 2017. The pixel values, shown in the grayscale inset, are expressed as band-averaged spectral radiances in units of $\mathrm{mW}/(\mathrm{m}^2\mathrm{sr}\,\mathrm{cm}^{-1})$. The Moon shape is elliptical due to the scan rate of the sensor as it sweeps across the Moon. (b) The reflectance (albedo) map, normalized to unity, was assembled from images taken by the DoD/NASA Clementine probe in 1994 with improvements made by the U.S. Geological Survey in 2009.

The full radiometric map has dimensions of 92160×46080 pixels but was downsampled to 2182×1091 pixels to allow for more efficient processing.

The AIF algorithm has the following steps.

1. Determine the position and elliptical shape of the Moon in the ABI image.
2. Find the coordinates of the pixel in the Clementine reflectance map that correspond to the center of the Moon in the ABI image.
3. Determine the rotational difference between the images.
4. Using the above information, project the radiometric Clementine map to the position, rotation, and shape of the ABI Moon.
5. Correct for interpolation errors and spectral differences to create a quasiflat field.
6. Divide the quasiflat field from the ABI image.

These steps are described in greater detail in the following sections.

2.1 *Elliptical Solution*

To facilitate the projection of the Clementine map to match the ABI image, the shape, size, and location of the ABI Moon must be determined. The image position of the ABI Moon changes for different bands and image captures; therefore, this calculation is required to be performed each time. These quantities can be measured with sufficient accuracy from empirical measurements using a curve fit to an ellipse. Following an approach similar to Wang et al.,[6] we apply

1. Sobel 45- and 135-deg edge detection functions to isolate the lunar rim.
2. A threshold filter to remove outliers and portions of the rim that fall into shadow.
3. A nonlinear least-squares fitting function for an ellipse to determine the center and semiaxis locations.[17]

The fit results are verified visually by overlaying the calculated ellipse onto the image. The ABI image is stretched in the direction of the minor axis by the ratio of the major axis to the minor axis to form a spherical projection of the Moon. This image of a spherical moon, shown in Fig. 2(a), becomes the control image for determining the corresponding pixel (CP) and rotation difference. A spherical projection of the Clementine image is shown in Fig. 2(b).

2.2 *Corresponding Pixel and Rotation*

The process requires the coordinates of the pixel in the rectangular Clementine map that correspond to the center pixel of the spherically projected ABI Moon and the relative orientation

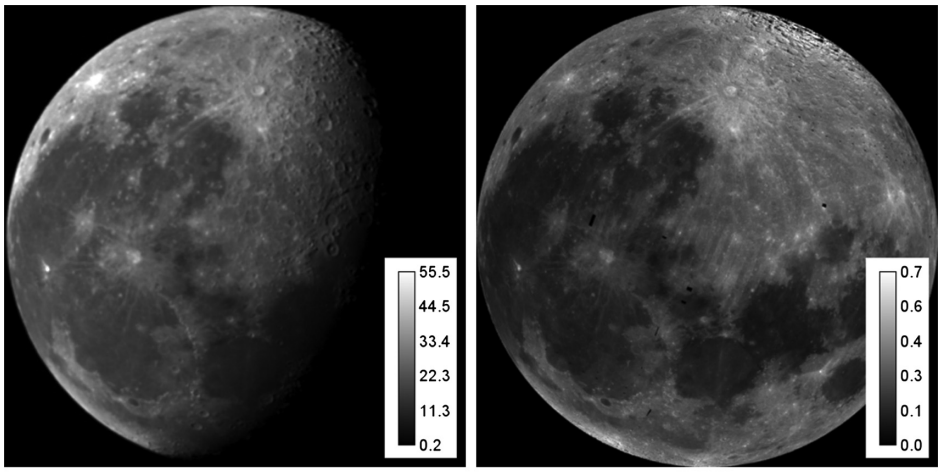

Fig. 2 Spherical projection of (a) the ABI image and (b) the Clementine reflectance map.

difference. It is possible that the selenographic coordinates of the center pixel location in the ABI Moon image can be calculated by knowing the relative rotation of the Moon and the relative coordinates between the Moon and the GOES satellite. This information was not available during the development of this approach, but it could be appropriate to calculate if this approach becomes common practice. Alternatively, we created an iterative process that searches an area of the Clementine map to find the coordinates that will produce the best correspondence. The search area on the Clementine map is typically a 64×64 pixel region surrounding an initial midpoint determined by visual comparison of the nonshaded lunar features in the two images. This region of interest can be made smaller with increased confidence in the position of the CP. One could also use the selenographic coordinates of primary lunar features to triangulate the position of the center pixel in the ABI image, but we found that visual inspection is sufficient for the current work. Even with advance knowledge of the coordinates, phase correlation or similar image registration methods would be necessary to achieve subpixel accuracy.

This computation takes a few hours on a desktop computer and has the following steps.

1. For each pixel in the Clementine search area, the rectangular Clementine image is projected onto a sphere centered on the specified pixel.
2. A log-polar phase correlation[18] is used to compare the spherical Clementine image with the spherical ABI image. The resulting correlation peak is unique to the Clementine pixel coordinates and provides information about the amount of rotation and scale difference between the images. The correlation peak amplitude provides the level of confidence in the match.
3. The correlation peak amplitude and calculated rotation are mapped for each pixel in the search area.
4. The best CP is identified with subpixel accuracy as the location of the maximum value in the correlation peak map.
5. The rotation is found at the same coordinates on the rotation map.

The phase correlation method is described by Reddy and Chatterji.[18] To achieve measurement of rotation (and scale if desired) difference, the images are remapped, in image space, such that the vertical axis represents the angle of the pixel coordinates and the horizontal axis represents the radius of the pixel coordinates before the phase correlation is applied. The polar transformation of the ABI image and the spherical Clementine image are shown in Figs. 3(a) and 3(b), respectively. It is worth noting that a primary difference between the images is a translational shift. The amount of shift is determined by the application of phase correlation[18] between the polar-mapped images, and the translation corrections are converted into rotation and scale for each loop. When the pixel in the search area is close to the CP, the scale difference calculated

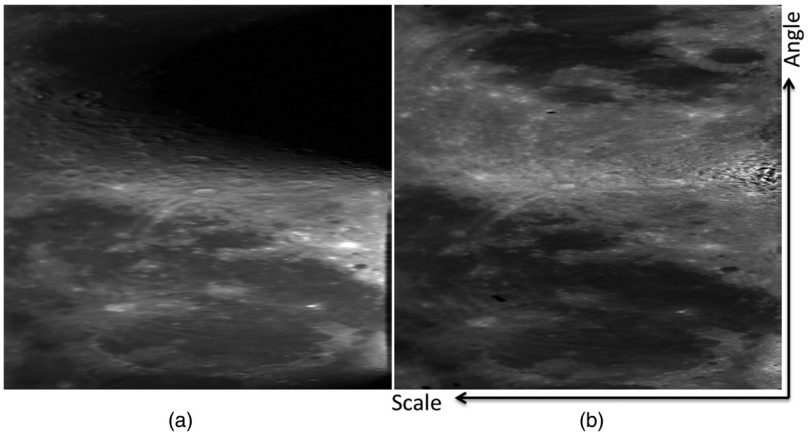

Fig. 3 Polar transformations of (a) the spherical ABI image and (b) the spherical Clementine image. The vertical axis is rotation, and the horizontal axis is scale. Application of phase correlation produces a measurement of the rotation and scale differences between the images.

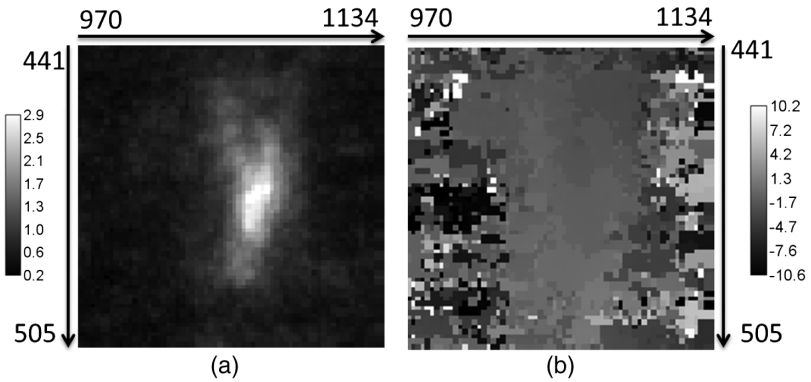

Fig. 4 (a) A 64 × 64 correlation peak map and (b) rotation map produced point-by-point by performing a polar phase correlation between the spherical Clementine image and ABI image over the search area. The horizontal and vertical axes refer to the pixel coordinates in the Clementine reference map. The grayscale bar on the left shows pixel values that correspond to the correlation peak amplitude. The grayscale bar on the right indicates the rotation angle (deg) necessary to align the Clementine image to the ABI image.

from the phase correlation will be negligible. The calculated rotation difference at the CP in this case was 6.34 deg.

As mentioned, the correlation peak amplitude is recorded for every pixel of the search area, thereby producing a correlation map, as shown in Fig. 4(a). For each location, there is a corresponding rotation [Fig. 4 (b)] and scale difference (not shown). To find the CP, the maximum value is located in the correlation map using a centroid to achieve subpixel accuracy.[19]

2.2.1 *Spectral and interpolation correction*

There is a difference in the spectral range of the Clementine image, centered at 750 nm, and the ABI (band 1) image, centered at 481 nm. The difference primarily affects the processing of the sea regions that appear darker when the ABI wavelength is lower than the Clementine image. This effect can be counteracted by applying a simple photographic gamma function spectral albedo model in the form of $I(m,n)^{\gamma}$ to the Clementine projection. For each reflective ABI band (bands 1 to 6), the applied gamma value is determined empirically by multiple applications of the method while varying the gamma value. A sufficient value is found when the difference between sea regions and nonsea regions is minimized. This can be accomplished programmatically, but we found that visual inspection is sufficient to determine appropriate gamma values. For bands 1 to 6, the gamma values are 0.6110, 0.6140, 0.6485, 0.5735, 0.5660, and 0.5375, respectively. It is certainly possible to use calibrated radiance values to quantitatively match the ABI and projected Clementine images, but this is complicated by the mismatch in spectral bands of the two imagers. One needs to factor in the center wavelength and width of the bands and make corresponding adjustments to portions of the Moon according to the spectral reflectance. The flat field and resulting edge response function are normalized. As such, quantitative irradiance values do not affect the calculation of the spatial resolution.

Interpolation of the images can produce artifacts in the MTF. As such, the procedure was designed to avoid interpolations applied to the target image. After a spherical Clementine Moon is found to match the spherical ABI Moon, the Clementine image is interpolated to match the shape and position of the original ABI image. Interpolation of the Clementine image, however, can produce errors at the lunar edge where there is no information. To compensate for this issue, an image with all unity values that has the same dimensions as the Clementine map is created. All operations that are applied to the Clementine map are also applied to this "white" image. Pixels on this white image are mostly unaffected by the interpolations with the notable exception of diminished values along the elliptical rim. The Clementine projection is divided by this correction image to compensate for the interpolation artifacts.

3 Results

Figure 5(a) shows an original GOES-16 band 1 ABI image and the result after AlF. Large-scale features have been successfully flattened, while, as a result of the difference in spatial resolutions of the images, small-scale features are still visible. Some features may also be attributed to shadows produced by the difference in view angle as the Clementine map was created from a mosaic of mostly nadir views of the Moon. Images from GOES-17 band 1 are shown in Fig. 6. Small diagonal stripes are apparent at the center of these images. The stripes result from an artifact in the mosaic of the Clementine image and could affect the results if the stripes appear near the edge of the Moon. Flattened images from other bands are shown in Figs. 7 and 8.

ESFs are taken from a series of rows near the left-most edge of the Moon, ranging from 50 pixels to the left of the edge and extending to 50 pixels to the right. The cases used for this paper demonstrate the difficulty of obtaining a step-like function, depending on the topography of the Moon near the edge. For the GOES-16 image, the edge of the Moon lies just beyond

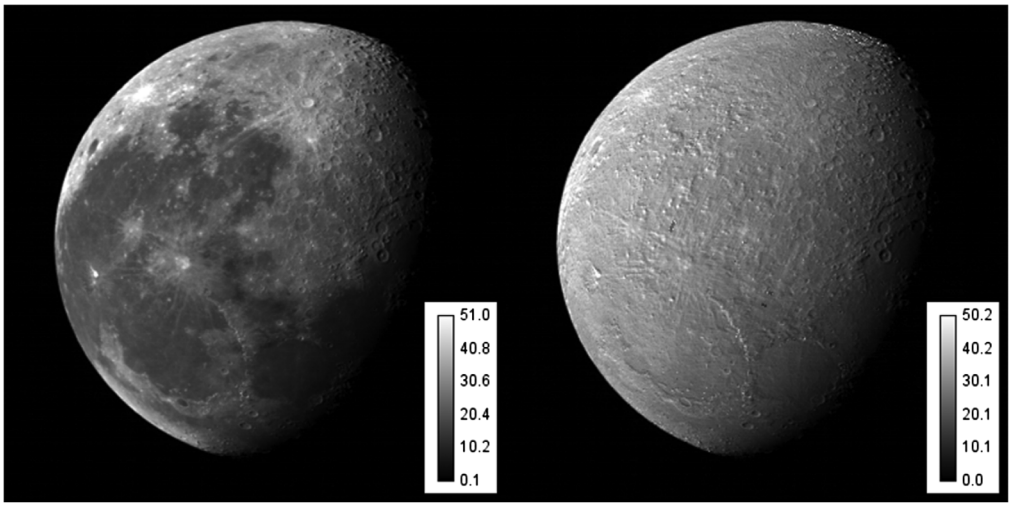

Fig. 5 (a) The band 1 ABI lunar image from GOES-16. (b) The image after division by a correction image created from the Clementine reflectance map.

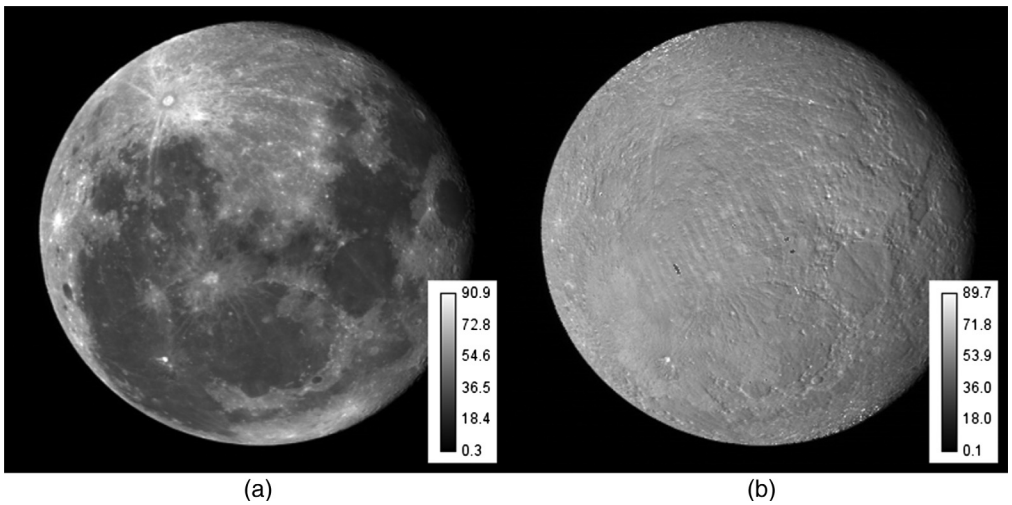

Fig. 6 (a) The band 1 ABI lunar image from GOES-17. (b) The image after division by a correction image created from the Clementine reflectance map.

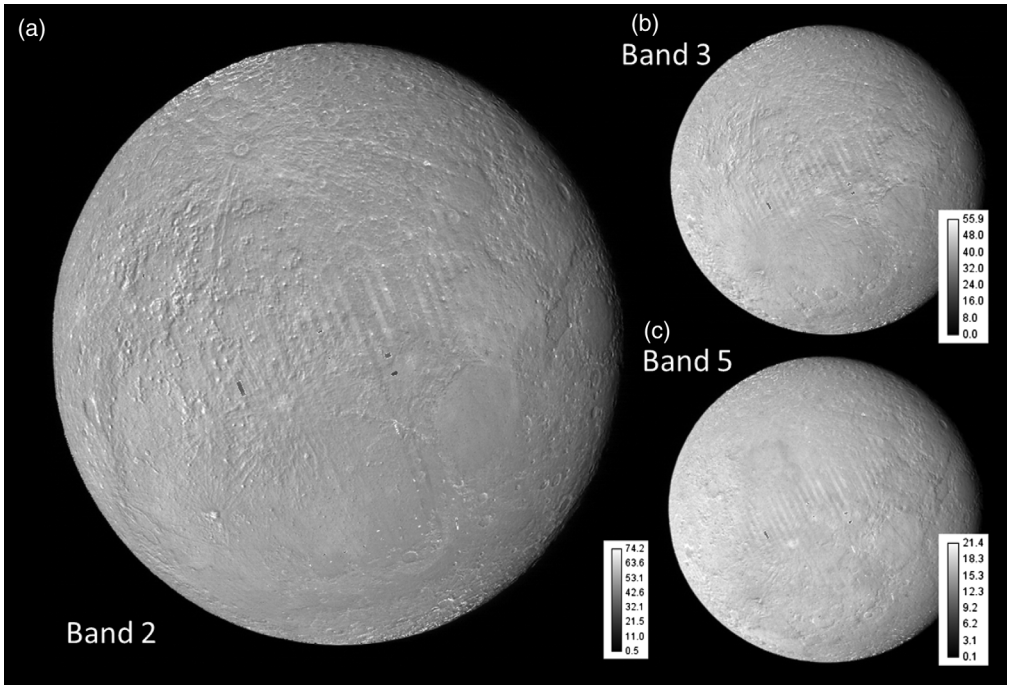

Fig. 7 Application of AIF to (a) band 2, (b) band 3, and (c) band 5 for GOES-17.

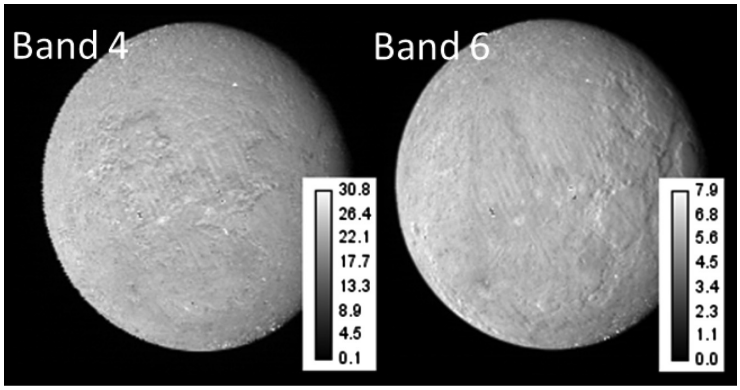

Fig. 8 Application of AIF to (a) band 4 and (b) band 6 for GOES-17.

the rim of the dark region Oceanus Procellarum. For the GOES-17 image, the desired line-out runs across the bright Byrgius crater. Figure 9 shows profile plots taken from a single row extending from the left of the Moon to the center, comparing original and processed band 1 images from each satellite.

3.1 *Edge Spread Functions*

With flattened images, ESFs can be taken from the corrected ABI images. With a single line-out, there are an insufficient number of data points to define a good ESF. Instead, several rows surrounding the midpoint are combined by shifting the edge position in each row to be aligned with subpixel accuracy. These shifts can be calculated if the elliptical shape is known with high accuracy, but this is complicated by the digital sampling of the slightly curved edge. We measured the shifts by fitting a sigmoid function with a ramp, modeling the edge, to each row to obtain the position of the edge using the following equation:

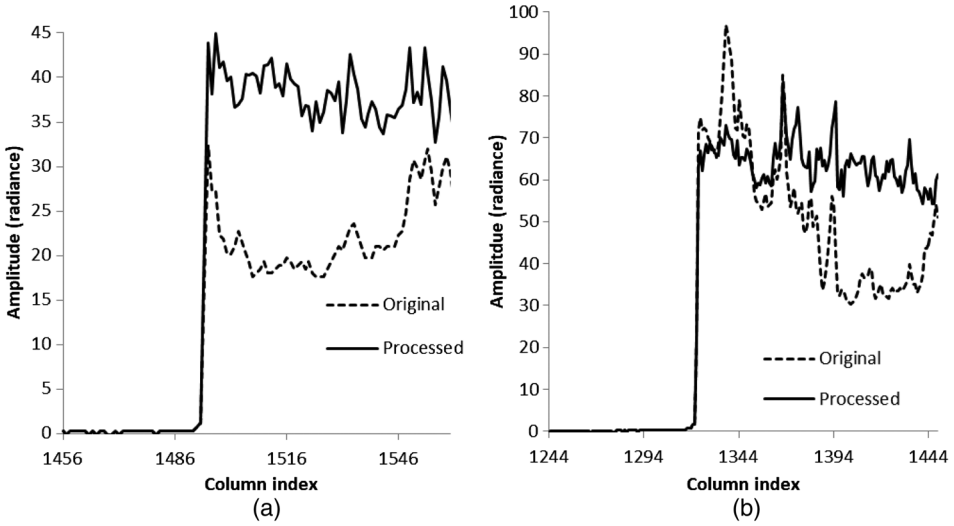

Fig. 9 Representative profile plots from an original ABI image (dotted) and the albedo-corrected image. The data on the left are from Fig. (5). The data on the right are from Fig. (6).

$$F(x) = [a_0 x + a_1]\left\{1 - \frac{1}{1 + \exp[-a_3(x - a_2)]}\right\}, \tag{1}$$

where the first factor is a linear equation with a slope a_0 and offset a_1 describes the shading. The second factor is the sigmoid function, where a_2 defines the edge position and a_3 expresses the amount of curvature at the edge.

After the data are aligned and combined, a final fit of Eq. (1) is applied to derive a continuous curve from the data points to serve as the ESF. The fit is applied to 50 data points, as opposed to pixels, on each side of the curve. The pixel distance for 100 points is about 4.8 pixels for band 1. There is no significant change in the final measurement when more points are included, but with fewer points, the goodness-of-fit value χ^2 starts to increase. Figure 10(a) shows the alignment of 16 rows that surround the midrow of the Moon and a successful final curve fit. The downward slope to the right of the edge stems from the $(a_0 x + a_1)$ portion of the fitting function. For comparison, the same process was applied to the original ABI without AlF, and as shown in Fig. 10(b), the curve fit fails. Figure 11 shows a similar example from GOES-17 band 1.

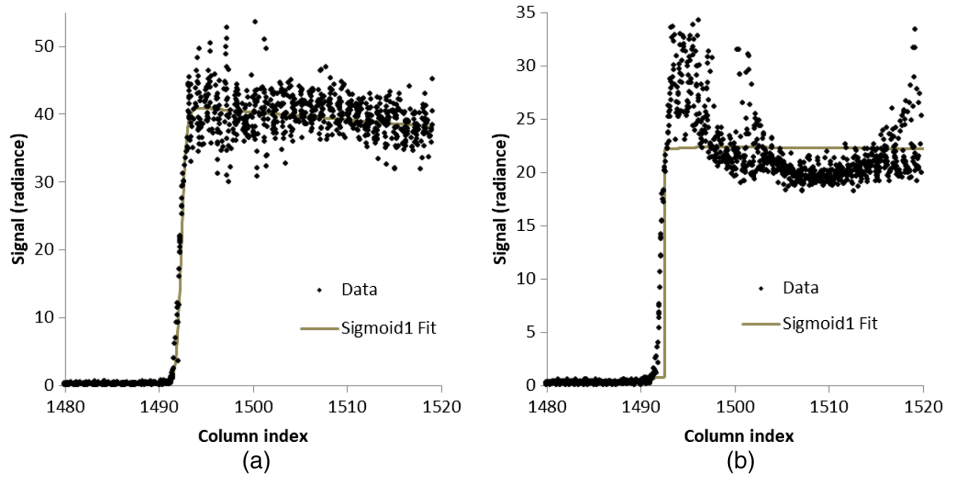

Fig. 10 (a) Alignment and fit to 16 rows near the image equator for band 1 on the albedo-flattened image. (b) Applying the same procedure to the original ABI produces the data and a failed fit.

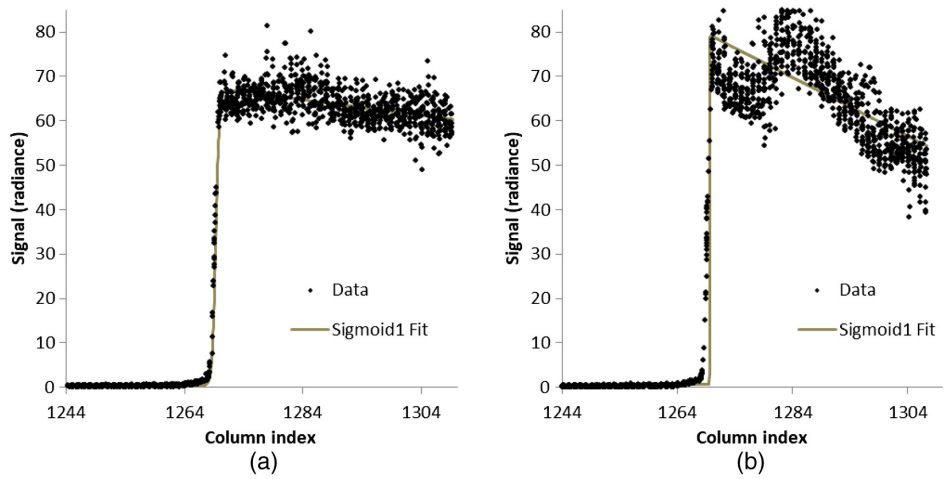

Fig. 11 (a) Alignment and fit to 24 rows near the image equator for band 1 on the albedo-flattened image from GOES-17. (b) Applying the same procedure to the nonflattened ABI image produces the data and a failed fit.

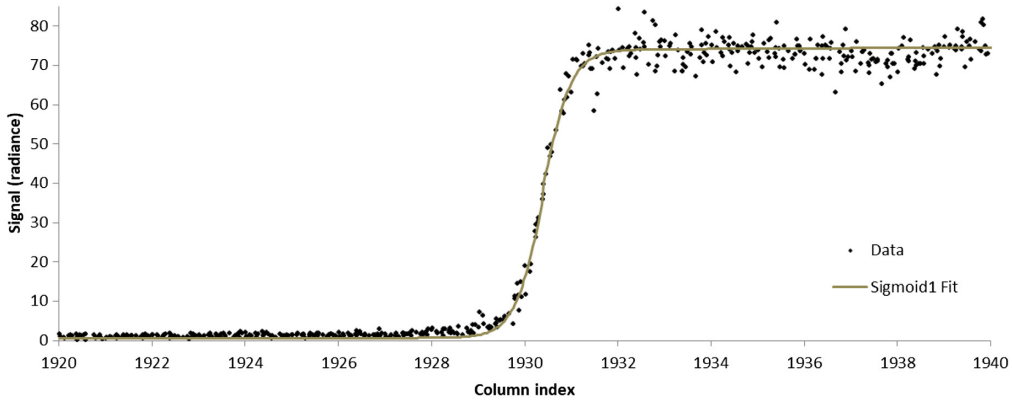

Fig. 12 An expanded view of the edge spread data and sigmoid fit applied to GOES-17 band 2.

Other functions, such as the Fermi function[20] and Cauchy function,[21] were considered, but we found that the sigmoid function produced a better fit to our data. After application of AIF, variations due to lunar features were diminished, resulting in a comparatively well-behaved data set. As such, no additional filtering was required to apply the fitting function to the edge spread data. Figure 12, an expanded view of the edge spread data for GOES 17, band 2, demonstrates the quality of the fit to a Sigmoid function.

The line spread function is created by taking the derivative of the ESF with the ramp factor removed. The MTF is calculated by taking the magnitude of the FFT of the line spread function and normalizing to unity.

MTF values for the four key spatial resolutions are shown in Tables 1 and 2. These values are measured from the eastern edge of the Moon while the ABI camera is scanning in the east–west (EW) direction. The column headers refer to the spatial resolution as a fraction of Nyquist, a common method for displaying the results. For bands 1, 3, and 5, the values are 4500, 9000, 13,500, and 18,000 cycles per radian. For band 2, the values are 9000, 18,000, 27,000, and 36,000 cycles per radian. For band 4 and 6, the values are 2250, 4500, 6750, and 9000 cycles per radian. The right-most column shows the number of images used to create the average values.

The last rows of Tables 1 and 2 show the MTF requirements as described in the GOES-R Mission Requirements Documents for level 1b images, while our process was applied to level 1α (detector pixel) images. MTF analysis on level 1b images is dependent on the interpolation method required to fit the image to the Earth-based fixed grid. The method applied to our data

Table 1 GOES-16 ABI average spatial resolution and standard deviations in terms of MTF for the four criterion points. The last column shows the number of images used to create the information. All measurements exceeded requirements.

		Average				Standard deviations				
Band	λ (μm)	Nyq/4	Nyq/2	3Nyq/4	Nyq	Nyq/4	Nyq/2	3Nyq/4	Nyq	Number
1	0.47	0.971	0.884	0.764	0.625	0.005	0.020	0.038	0.053	5
2	0.64	0.946	0.807	0.632	0.448	0.009	0.028	0.045	0.052	5
3	0.87	0.966	0.874	0.745	0.594	0.006	0.020	0.035	0.049	6
4	1.38	0.954	0.823	0.651	0.482	0.004	0.010	0.017	0.021	6
5	1.61	0.940	0.785	0.595	0.419	0.005	0.010	0.014	0.015	6
6	2.25	0.958	0.833	0.669	0.508	0.012	0.048	0.084	0.105	6
Requirements	—	0.900	0.730	0.530	0.320	—	—	—	—	—

Table 2 GOES-17 ABI average spatial resolution and standard deviations in terms of MTF for the four criterion points. All measurements exceeded requirements.

		Average				Standard deviations				
Band	λ (μm)	Nyq/4	Nyq/2	3Nyq/4	Nyq	Nyq/4	Nyq/2	3Nyq/4	Nyq	Number
1	0.47	0.954	0.836	0.685	0.534	0.018	0.061	0.103	0.129	4
2	0.64	0.954	0.807	0.617	0.462	0.006	0.021	0.034	0.039	7
3	0.87	0.955	0.812	0.651	0.470	0.002	0.009	0.014	0.017	3
4	1.38	0.955	0.817	0.651	0.475	0.003	0.018	0.018	0.028	4
5	1.61	0.948	0.792	0.610	0.472	0.003	0.010	0.018	0.015	4
6	2.25	0.950	0.819	0.622	0.460	0.006	0.017	0.030	0.034	4
Requirements	—	0.900	0.730	0.530	0.320	—	—	—	—	—

set sharpened the edge feature, resulting in higher MTF values than calculated from level 1α images and a nonreal artifact at the base of the edge. This prompted the decision to apply the method to level 1α images concluding that if the MTF values from level 1α images exceed the requirements, then it is safe to state that the current state of the imaging system exceeds the requirements.

The values in Table 1 are significantly higher than the EW results reported by Wilson and Xiong[9] but are similar in range with their north–south (NS) results. The authors leave the discussion of the discrepancy between their EW and NS results to future work, but we suspect that the inconsistency stems from the application of their method to level 1b images that have been interpolated in the EW direction. Application of interpolation to an image changes the MTF derived from the image.[22] Other discrepancies can be attributed to differences in methodology for obtaining the MTF and using AlF to produce more consistent ESFs.

An attempt was made to compare the variation between MTF measurements made with and without the application of AlF. Table 3 shows the result from GOES-16 band 1 for images taken on January 1, 2017, and February 2, 2017, which differ in the lunar features that appear on the eastern edge. With AlF, the results are consistent with the average displayed in Table 1. Without flattening, the near-edge features produced broken curve fits, similar to Fig. 10, resulting in abnormally high values for the MTF.

Table 3 Comparison of MTF resolution for two GOES-16 captures with and without AIF.

Day	AIF	Nyq/4	Nyq/2	3Nyq/4	Nyq
January 15, 2017	No	0.990	0.977	0.973	0.959
January 15, 2017	Yes	0.970	0.875	0.740	0.592
February 17, 2017	No	0.987	0.949	0.891	0.809
February 17, 2017	Yes	0.974	0.901	0.797	0.663

4 Conclusion

We have presented the AIF method to improve the reliability of spatial resolution measurements for Earth-viewing satellites when an edge response function is derived from the lunar edge. A reflectance (albedo) map from the Clementine mission was aligned to images of the Moon taken by the NOAA/NASA GOES-16 and GOES-17 satellites using repeated applications of phase correlation to obtain the difference in both location and rotation. The Clementine image was remapped to act as a flat-field image for the Moon's albedo. Division of the original image by the Clementine correction image effectively removed large-scale features from the ABI image, producing a more consistent step-like function at the lunar edge. This has been applied to all nonemissive bands, as shown in Figs. 7 and 8. Although the method requires significantly more computations than conventional approaches, the results are more reliable.

Acknowledgments

This study was supported through the NASA GOES-R Program, ABI Flight Project. The contents are solely the findings of the authors and do not constitute a statement of policy, decision, or position on behalf of NOAA, NASA, or the U.S. Government.

References

1. S. E. Reichenbach, S. K. Park, and R. Narayanswamy, "Characterizing digital image acquisition devices," *Opt. Eng.* **30**(2), 170–177 (1991).
2. J. Li et al., "Efficient assessment method of on-board modulation transfer function of optical remote sensing sensors," *Opt. Express* **23**(5), 6187–6208 (2015).
3. N. R. Nelson and P. S. Barry, "Measurement of Hyperion MTF from on-orbit scenes," in *IEEE Int. Geosci. and Remote Sens. Symp.*, Vol. 7, pp. 2967–2969 (2001).
4. K. Buskila et al., "Atmospheric modulation transfer function in the infrared," *Appl. Opt.* **43**(2), 471–482 (2004).
5. J. J. Shea, "Lunar limb knife-edge optical transfer function measurements," *J. Electron. Imaging* **8**(2), 196–208 (1999).
6. Z. Wang et al., "On-orbit characterization of MODIS modulation transfer function using the Moon," *IEEE Trans. Geosci. Remote Sens.* **52**(7), 4112–4121 (2014).
7. P. Mahanti et al., "In-orbit multi-spectral image sharpness assessment for the lunar reconnaissance orbiter wide angle camera," in *IEEE Aerosp. Conf.*, IEEE, pp. 1–8 (2014).
8. G. R. Keller, T. Chang, and X. Xiong,"MTF analysis using lunar observations for Himawari-8/AHI," *Proc. SPIE* **10402**, 104022I (2017).
9. T. Wilson and X. Xiong, "Modulation transfer function characterization for GOES-16 Advanced Baseline Imager using lunar observations," *Proc. SPIE* **11127**, 111271Y (2019).
10. H. H. Kieffer and T. C. Stone, "The spectral irradiance of the Moon," *Astronom. J.* **129**(6), 2887–2901 (2005).
11. S. Nozette et al., "The Clementine mission to the Moon: scientific overview," *Science* **266**(5192), 1835–1839 (1994).
12. T. J. Schmit et al., "A closer look at the ABI on the GOES-R series," *B Am. Meteorol. Soc.* **98**(4), 681–698 (2017).

13. S. Kalluri et al., "From photons to pixels: processing data from the Advanced Baseline Imager," *Remote Sens.* **10**(2), 177–215 (2018).
14. J. F. Kordas et al., "UV/visible camera for the Clementine mission," *Proc. SPIE* **2478**, 175–186 (1995).
15. E. M. Lee et al., "A new Clementine basemap of the Moon," in *Lunar and Planetary Sci. Conf. XL*, Houston, Texas (2009).
16. B. A. Archinal et al., "A Clementine derived control network and topographic model—the unified lunar control network 2005," in *IAU Joint Discussion*, Vol. 10, p. 26 (2006).
17. C. B. Markwardt, "Non-linear least-squares fitting in IDL with MPFIT," *Astron. Data Anal. Softw. Syst.* **XVIII 411**, 251–255 (2009).
18. B. S. Reddy and B. N. Chatterji, "An FFT-based technique for translation, rotation, and scale-invariant image registration," *IEEE Trans. Image Process.* **5**(8), 1266–1271 (1996).
19. J. N. Caron, M. J. Montes, and J. L. Obermark, "Extracting flat-field images from scene-based image sequences using phase correlation," *Rev. Sci. Instrum.*, **87**(6), 063710 (2016).
20. T. Choi, X. Xiong, and Z. Wang, "On-orbit lunar modulation transfer function measurements for the Moderate Resolution Imaging Spectroradiometer," *IEEE Trans. Geosci. Remote Sens.* **52**(1), 270–277 (2013).
21. T. Li and H. Feng, "Comparison of different analytical edge spread function models for MTF calculation using curve-fitting," *Proc. SPIE* **7498**, 74981H (2009).
22. A. Ahmed et al., "Residual interpolation for division of focal plane polarization image sensors," *Opt. Exp.* **25**(9), 10651–10662 (2017).

James N. Caron is a principal research scientist at Research Support Instruments in Lanham, Maryland, USA. He received his BS degree in physics from Michigan State University in 1990 and his MS degree and PhD in physics from the University of Delaware in 1995 and 1997, respectively. He has authored 15 journal papers and 30 conference papers and holds three U.S. patents. His current research interests include laser-based ultrasound detection of dark matter, advanced Fourier-space image processing, laser ultrasound, and calibration of remote sensing systems. He is a senior member of the Optical Society.

Chris J. Rollins is a vice president of Research Support Instruments in Lanham, Maryland, USA. He received his PhD in physics from Northeastern University in 1984. He has performed systems engineering and optical design for the Naval Research Laboratory (NRL) Clementine mission, the NRL-HSI hyperspectral satellite, and TacSat-4. He is currently the ABI Flight Project Instrument Systems Engineer and represents the ABI Flight Project on the GOES-R Calibration Working Group.